Interdisciplinary Research Review
Volume 15, Number 1, Pages 1 – 8

Performance evaluation of wavelet time-resolved phase-amplitude coupling estimates on small numbers of trials

Sopapun Suwansawang*

Faculty of Science and Technology, Nakhon Pathom Rajabhat University, Nakhon Pathom 73000, Thailand

Abstract

Time-resolved phase-amplitude coupling (tPAC) is increasingly used in clarifying the interactions between neuronal oscillation of different frequencies. In this study, Airy wavelet-based method for tPAC estimates on small numbers of trials is presented. The method was validated using both synthesized and experimental data. Simulation results suggested that tPAC analysis using more than 15 trials offers better joint time-frequency resolution. Experimental results showed that tPAC estimates on 30-, 50-, and 100-step cycles are able to detect similar significant coupling in the time-frequency plane. Dominant couplings are between ≈ 6 Hz and 8-32 Hz around heel contact. These frequency components partly overlap with the frequency components of motor unit activity during human treadmill walking. Wavelet tPAC analysis presented in this study may be used to track time-localised common oscillations in short segments of non-stationary neurophysiological signals with varying time and frequency resolution.

Keywords: Cross-frequency, non-stationary analysis, Morse wavelet, signal processing.
Article history: Received 2 December 2019 Accepted 21 February 2020

1. Introduction

Signal processing has become increasingly important in the field of neuroscience [1 – 4]. Analysis of the frequency content of electrophysiological signals are useful ways to examine neuronal synchrony [1, 5]. A broad class of neurophysiological signals may be modeled as modulated oscillations, using analytic signals. Continuous complex-valued wavelet transforms play a key role in analysis of modulated oscillatory signals [6]. In recent years, analytic continuous wavelet transform − generalized Morse wavelets, have become a popular time-frequency analysis technique [7 –10]. They are highly flexible and form a two-parameter family of wavelets that have been used for studying time-varying properties of non-stationary neurophysiological signals [7, 11].

There are a number of popular measures used to investigate and characterise non-stationary neuronal coupling. Recently, there is increasing interest in clarifying the interactions between neuronal oscillations of different frequencies [11 – 16]. This form of interaction is commonly called cross-frequency coupling (CFC). One type of CFC, known as phase-amplitude coupling (PAC) or nested oscillation, occurs when the amplitude of a high frequency oscillation is modulated by the phase of a low frequency oscillation. More recently, several methods have been used to evaluate PAC on electrophysiology recordings such as electroencephalogram (EEG), local field potential (LFP) and other brain recordings [11, 14, 15, 17 – 22]. Most methods investigate PAC in the frequency domain and require long segments of experimental data. Recently, a time-resolved measure of phase-amplitude coupling (tPAC) between neural oscillation is used to detect temporal profile and frequencies of coupled oscillatory components [22]. The study of [22] suggests that tPAC provides high temporal resolution, the capacity of estimating coupling strength, and low sensitivity to noise conditions obtained with the short data lengths.

This paper focused on the application of wavelets and spectral tracking methods. The aim was to develop techniques that characterise short segments of data from natural movements. The behaviour of the generalised Morse wavelets-based method for tPAC analysis with an emphasis on small numbers of trials was explored. Our method was validated using both simulated and experimental data. We concluded with a discussion of our approach and recommendations regarding the current findings.

*Corresponding author; email:sopapun@webmail.npru.ac.th

DOI: 10.14456/irr.2020.1

2. Methods

2.1. The generalized Morse wavelets

The generalized Morse wavelets are complex-valued analytic wavelet transforms containing information on both amplitude and phase [6]. They are maybe a good choice for application to very time-localized structures [23, 24]. The generalised Morse wavelets form a two-parameter family of wavelets, β and γ. By varying these two parameters, the generalised Morse wavelets can take on a wide range of characteristics and still remain exactly analytic. The analyticity of wavelets ($\Psi(\omega) = 0$ for $\omega < 0$) is important for the analysis of strongly modulated signals, where the wavelets are required to be very narrow in time for matching the modulation time scale [23].

The zero order generalized Morse wavelet used in this study is defined in frequency domain as

$$\Psi_{\beta,\gamma}(\omega) = \sqrt{2}H(\omega)A_{k;\beta,\gamma}\omega^{\beta}e^{-\omega^{\gamma}} \tag{1}$$

where $H(\omega)$ is the Heaviside unit step function and $A_{k;\beta,\gamma}$ is a normalising constant that can be expressed by

$$A_{k;\beta,\gamma} = \sqrt{\pi\gamma 2^{r}\Gamma(k + 1/\Gamma(k + r))} \tag{2}$$

where $\Gamma(\bullet)$ denotes the gamma function and $r = (2\beta + 1)/\gamma$. The maximum amplitude occurs at the peak frequency [8],

$$\omega_{\beta,\gamma} \equiv \left(\frac{\beta}{\gamma}\right)^{\frac{1}{\gamma}} \tag{3}$$

The rescaled second derivative of the frequency-domain wavelets evaluated at its peak frequency is $P^2_{\beta,\gamma} \equiv \beta\gamma$, and $P_{\beta,\gamma}$ is called the dimensionless wavelet duration [6], defined as

$$P_{\beta,\gamma} \equiv \sqrt{\beta\gamma} \tag{4}$$

It is worth to note that Eq. (3) and (4) are key properties which depend only on two parameters, β and γ.

To explore the trade-off between time and frequency precision, the localisation measures (σ_t, σ_ω, $A_{\beta,\gamma}$, and $P^2_{\beta,\gamma}$) for some members of the generalized Morse wavelets are given in Table 1. Note that σ_t and σ_ω are a time width and a frequency width of the window function or a standard deviation (radius) in time and frequency of the wavelet, respectively. This table provides alternative choices for a particular application. For example, at fixed $P^2_{\beta,\gamma} = \beta\gamma = 12$, the Heisenberg area of $\gamma = 3$ is the most close to its lower bound for $\beta > 1$, as seen in Table 1. More details regarding the different roles of β and γ in controlling wavelet properties can be found in [6, 8, 23].

In summary, Airy wavelets ($\gamma = 3$) are desirable in this study because they give wavelets having a high degree of symmetry in the frequency domain, as seen in Table 1. Increasing β ($\beta > 3$) at γ= 3, the Heisenberg area of the generalized Morse wavelets ($A_{\beta,\gamma}$) approaches its theoretical lower bound at $A_{\beta,\gamma}$=0.5. This property may lead to good performance as previously mentioned. Increasing β at fixed γ, wavelets are more oscillatory and have a narrower bandwidth in the frequency domain. Generally, choosing a small value of β gives wavelets that are highly time-localized as opposed to frequency-localized, as seen in Table 1 for the values of σ_t and σ_ω. Note that with $\gamma = 3$, β should be grater than one ($\beta > \left(\frac{\gamma-1}{2}\right)$), as stated in [24].

2.2. Wavelet time-resolved phase-amplitude coupling estimates

Time-resolved PAC (tPAC) is a method to resolve PAC measures in time. Here, an estimation of tPAC in time-frequency map adapted from [22] and [25] can be calculated by

$$tPAC = \frac{1}{N}\sum_{n=1}^{N}\left(\frac{|Z_{f_A,f_P,n}|}{\sqrt{\overline{A^2_{f_A}}}}\right) \tag{5}$$

where N is the number of trials, $\overline{A^2_{f_A}}$ is mean value of $A^2_{f_A}$, and Z_{f_A,f_P} is given by

$$Z_{f_P,f_A} = |A_{f_A}| \cdot e^{i\phi_{f_P}} \tag{6}$$

Eq. (6) could be used to extract a phase-amplitude coupling measure where A_{f_A} is the envelope of higher-frequency oscillations, and ϕ_{f_P} is the phase of lower-frequency oscillations.

In this study, steps in the computation of tPAC based generalized Morse wavelets is shown in Fig. 1. First, the instantaneous amplitude envelope of the higher-frequency oscillation and instantaneous phase of the lower-frequency oscillation were calculated by obtaining an analytic representation of the original signal using generalized Morse wavelets. Secondly, the instantaneous amplitude and phase were extracted from the analytic representation, and then calculated as the absolute value and the phase angle of the analytic signal, respectively. The principle of the tPAC procedure requires the steps as the f_P with strongest phase-amplitude coupling with f_A bursts in each trial is searched for automatically using a power spectrum estimate [22]. To determine the dominant frequency f^*_P; the power spectrum P_A was estimated and its peaks were extracted. Also, the power spectrum P_x was estimated, and was used for finding the highest peak in P_A that co-occurred with a peak in P_x. See [22] for more details.

2.3. Confidence limits for tPAC estimates

To determine statistical significance of tPAC estimates, surrogate data are generated following the approach of [22] and [26]. Here, the amplitude information (A_{f_A}) in each trial is first split into five blocks. Then, these blocks are randomly permuted to yield a surrogate dataset. Further, the phase and amplitude information of the original data are shuffled randomly

Table 1. The localisation measures for some members of the generalized Morse wavelets.

	$\gamma = 2$				$\gamma = 3$				$\gamma = 4$			
β	σ_t	σ_ω	$A_{\beta,\gamma}$	$P^2_{\beta,\gamma}$	σ_t	σ_ω	$A_{\beta,\gamma}$	$P^2_{\beta,\gamma}$	σ_t	σ_ω	$A_{\beta,\gamma}$	$P^2_{\beta,\gamma}$
1	1.732	0.337	0.583	2	2.062	0.258	0.531	3	2.287	0.228	0.522	4
3	1.483	0.347	0.514	6	2.194	0.229	0.501	9	2.706	0.186	0.503	12
4	1.464	0.348	0.510	8	2.280	0.220	0.501	12	2.884	0.174	0.503	16
6	1.446	0.350	0.506	12	2.418	0.207	0.500	18	3.168	0.158	0.502	24
10	1.433	0.351	0.503	20	2.616	0.191	0.500	30	3.581	0.140	0.501	40
20	1.423	0.352	0.502	40	2.923	0.171	0.500	60	4.243	0.118	0.501	80
30	1.420	0.353	0.501	60	3.123	0.160	0.500	90	4.691	0.107	0.500	120

Note: the formulas for σ_t, σ_f are given in [23] and an example code is available at http://site.google.com.site/aguiarconraria/joanasoares-wavelets/the-astoolbox.

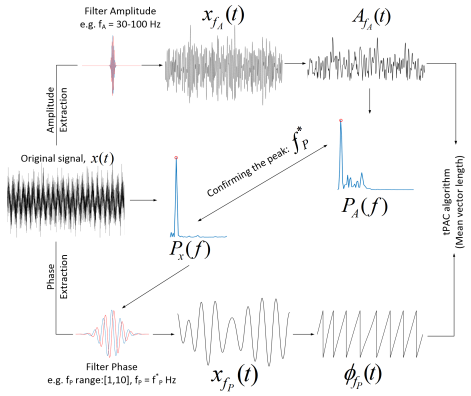

Figure 1: Graphical overview of tPAC method. Details are stated in text.

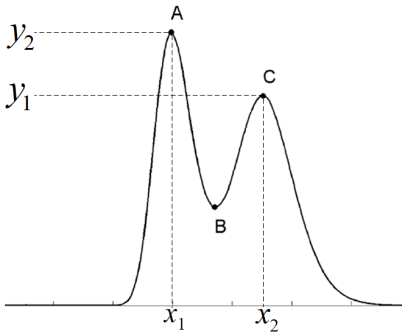

Figure 2: Plot showing criterion for spectral and temporal resolution adapted from [3].

between the different frequency components [27]. For each shuffled phase information obtained from the i^{th} frequency is randomly matched with the shuffled amplitude data from j^{th} frequency, where i and j are pseudorandom integers. The tPAC parameter estimates within the 95$^{\text{th}}$ percentile of the surrogate distribution are considered statistically significant.

2.4. Spectral and temporal resolution criteria

The test for spectral and temporal resolution is important in time-frequency analysis. Here, a measure of resolution based on the Rayleigh criterion and the study of [3] is used for performance evaluation of wavelet time-resolved phase-amplitude coupling estimates on each number of trials. Maximum resolution in the spectral and temporal domains is defined as minimum resolved frequency or interval for which conditions in Eq. (7) are true. Components x_1 and x_2 are resolved if normalized amplitude of coupling strength between the peaks B is less than half that of the lower of A and C which are defined in Fig. 2 [3].

$$Resolved(x_1, x_2) = \begin{cases} True : B < \frac{1}{2} min(A, C) \\ False : Otherwise \end{cases} \quad (7)$$

Additionally, we used Eq. (8), m, to recheck the performance of tPAC for testing the stability of temporal resolution. If m is high, tPAC measure is less stable in temporal resolution.

$$m = \frac{1}{Np - 1} \sum_{Np=1}^{Np-1} |y_2 - y_1| \quad (8)$$

where Np is number of peaks. y_2 and y_1 are defined in Fig. 2.

3. Application and results

3.1. General observations

In order to test the performance of the tPAC method using the generalized Morse wavelets, simulated data with controlled PAC parameters were used. It was generated using the method of [18] which was modeled as

$$x(t) = \overbrace{K_{f_P} \sin(2\pi f_P t)}^{x_{f_P}(t)} + \overbrace{A_{f_A}(t) \sin(2\pi f_A t)}^{x_{f_A}(t)} + \varepsilon(t) \quad (9)$$

where $\varepsilon(t)$ is additive noise, and

$$A_{f_A} = 0.5[K_{f_A}(1 - \chi) \sin(2\pi f_P t) + \bar{A}_{f_A}(t) + \chi + 1] \quad (10)$$

where $\bar{A}_{f_A}$ is a constant that determines the maximal amplitude of f_A, K_{f_P} and K_{f_A} are constant which determine the maximal amplitude of f_P and f_A, respectively. The parameter $\chi \in [0, 1]$ controls the intensity of the coupling: $\chi = 0$ represents maximum coupling while $\chi = 1$ is no coupling.

Here, the original signal was constructed with length of 2 s, sampling rate of 1000 Hz. Multiple modes of coupling in the study of [22] were applied for this testing, which were: during the first half of the signal (1 s), the phase of slow oscillation at f_{P_1} = 9 Hz was coupled to the amplitude of a faster oscillation at f_{A_1} = 115 Hz. In the second half, the first coupling mode was terminated and two other modes appeared simultaneously with f_{P_2} = 13 Hz, f_{A_2} = 145 Hz, f_{P_3} = 5 Hz, and f_{A_3} = 87 Hz, respectively. The signal-to-noise ratio was set to 6 dB, and the preferred coupling phase in the three modes were $\angle 270$, $\angle 0$, $\angle 180$, respectively. The coupling parameter (χ) in each mode were 0.5, 0.2, and zero, respectively. The frequency ranges of interest for f_P and f_A in the tPAC analysis were defined linearly as ranges $[1, 15]$ Hz and $[40, 200]$ Hz, respectively. The wavelet parameters, β was set to 3, 9 and 27. γ is 3. Here, tPAC analysis was calculated using averages over 100 trials.

Fig. 3 illustrates the tPAC analysis outcome on the synthesized data. Time-frequency maps reveal three coupling modes which there are areas of significant coupling between f_A=115 Hz and f_P=9 Hz during the time of 0-1 s, and the significant coupling between f_A=145 Hz, f_P=13 Hz and f_A=87 Hz, f_P=5 Hz occurred during the time of 1-2 s, as seen in tPAC coupling strength maps for f_A and f_P vs. time (Fig. 3(B)). The dominant coupling in each modes varied according to slow rhythm, for example, during the first half of the signal (1 s duration), the signal was averaged time locked to the troughs of the 9-Hz f_P cycle. Changing the value of β changes the frequency resolution of the corresponding wavelets. It is noticed that setting β to low value, the frequency resolution is decreased. Here, the results show that tPAC method is less accurate in detecting the coupling for β = 3. tPAC returns accurate results for setting value of β to 27, see Fig. 3(B)(top) compared to Fig. 3(B)(bottom). Note that time-frequency plots indicates values below the 95% confidence limit. Statistical significance test for tPAC is described in 2.3.

From the results given in this section, it has proved that tPAC method is more accurate in detecting the coupling for setting β to higher value. β = 27 and γ =3 may lead to good performance for time-frequency based tPAC analysis of simulated and experimental data in next section. The datasets used in the next section consist of different number of trials, which are 5, 15, 30, 50, and 100.

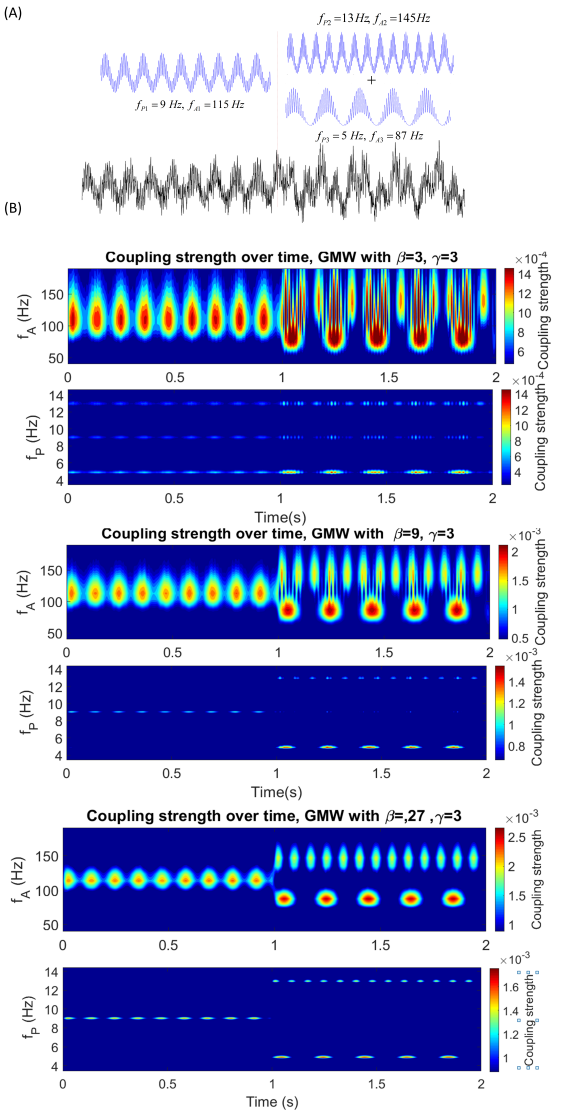

Figure 3: An example of tPAC analysis outcome on a synthesized data. (A) A synthesized data including three different coupling modes, see text for more details. (B) tPAC coupling strength maps for f_A and f_P vs. time. The 95% confidence limit for tPAC time-frequency plane is 0.47×10^{-3}.

3.2. *Results from simulated data*

Fig. 4(A) shows examples of the time-frequency tPAC analysis outcome on the simulated data calculated using averages over 5, 30, and 100 trials. The time-frequency maps illustrate the time course of all three coupling modes. The improved performances in coupling detection can be observed when using larger number of trials as clearly seen in Fig. 4(A)(middle and right). Interestingly, time-frequency maps of tPAC estimates from 30 trials and 100 trials seem to have a similar time-frequency resolution. To evaluate the performances of tPAC analysis in term of time-frequency resolution, Fig. 4(B-C) and Table 2 and 3 are presented. Fig. 4(B) and (C) shows examples of time- and frequency-varying normalized amplitude of coupling strength formed by cross-sectioning the time-frequency plane at three coupling modes. The plots for tPAC analysis using 5 trials display more variability in normalized amplitude of coupling strength when compared to the others. Also, only tPAC analysis using 5 trials is not deemed to be resolved according to above criteria. The plots of Fig. 4(B) and (C) show that tPAC analysis using number of trials between 30 and 100 trials give generally good time-frequency resolution.

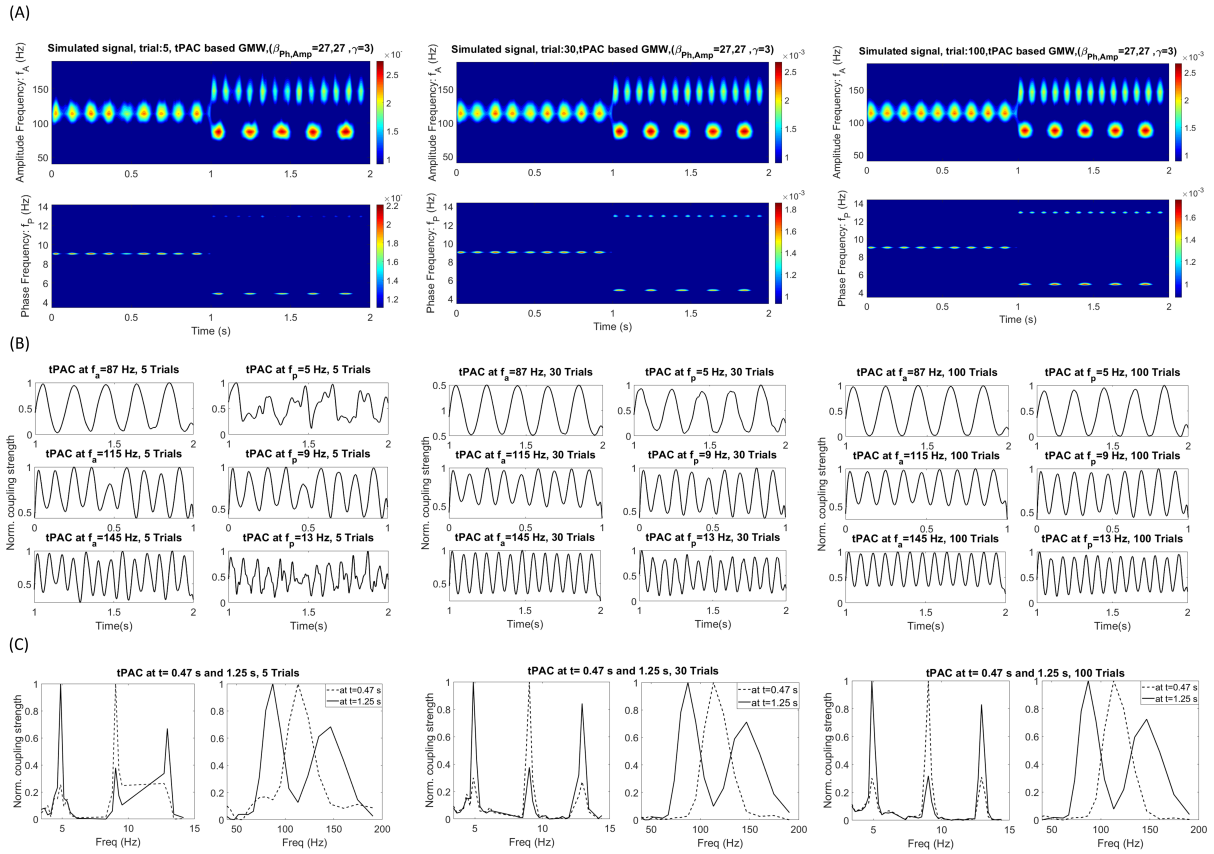

Figure 4: Examples of tPAC analysis outcome on a synthesized data calculated using averages over 5, 30, and 100 trials. (A) Plots showing time-varying normalized amplitude of coupling strength formed by cross-sectioning the time-frequency plane at three coupling modes, (f_P=5 Hz,f_A=87 Hz), (f_P=9 Hz,f_A=115 Hz), and (f_P=13 Hz,f_A=145 Hz). (B) Plots showing frequency-varying normalized amplitude of coupling strength formed by cross-sectioning the time-frequency plane at t=0.47 s and 1.25 s.

Table 2 lists the time resolution and the stability of time resolution, m of each number of trials when applied to the same simulated dataset used in Section 3.1. The table shows the maximum time resolution which is defined as the minimum resolved interval between adjacent bursts of signal using the method defined by Eq. (7) and Fig. 2. It can be seen that the time resolution and m of tPAC analysis using 5 trials performed slightly worse than using the other number of trials, especially at frequencies of 5 and 13 Hz, whereas in the other frequencies the time resolution and m do not decrease by more than 1 ms and 0.05, respectively. Table 3 lists the frequency resolution of tPAC analysis at each number of trials. It is interesting to note that the frequency resolution does not change by more than 5 Hz for any number of trials.

All results in this section would suggest that tPAC analysis using larger number of trials (> 15 trials) offers better joint time-frequency resolution.

3.3. Application to neurophysiology

The simulation procedure described above is repeated with experimental data. The data set analysed in this section comes from the study of [28]. This data set has been analysed and the novelty here is in application of time varying measures. The two EMG signals over the ankle flexor can be used as a substitute for pairs of motor unit recordings which can identify any modulation in the functional coupling during walking, and provide a basis for investigating the highly adaptive nature of human gait patterns [28]. EMG recordings were digitally sampled at rate of 1000 and 5000 Hz. Recordings were made over a period of 500 seconds. A contact switch identified heel strike. Thresholding of the heel strike (HS) record provides a sequence of trigger times. These trigger times provide a reference point within each step cycle which is used to segment the data for undertaking time-frequency analysis, where time is defined with respect to heel contact. Further details of experiments are given in [28]. The standard practice of rectification of surface EMG signals has been a commonly used pre-processing procedure that allows detection of EMG coherence [2] and was used here. EMG-EMG tPAC analysis was calculated using averages over 30-, 50-, and 100-step cycles. All steps were segmented into 1.04 s segments with 0.82 s before heel trigger and 0.22 s after heel trigger, as seen in Fig. 5(A). The time scale on time-frequency plots was labelled as 0-1.04 s, heel triggers are at 0.82 s in these plots. Thus, all plots cover swing phase including early, mid, and late swing for each step cycle. The EMG-EMG tPAC

Table 2. Temporal resolution and the stability of temporal resolution (in miliseconds; m) of each number of trials at each frequency.

Coupling freqs (Hz)	Number of trials				
	5	**15**	**30**	**50**	**100**
5	147;0.18	113;0.07	98;0.05	10;0.04	10;0.03
9	6.7;0.09	6.5;0.07	6.5;0.07	6.2;0.05	6.2;0.02
13	11;0.12	5.3;0.08	4.7;0.07	4.7;0.06	4.7;0.03
87	12.5;0.02	11;0.01	11;0.01	11;0.01	11;0.01
115	7.7;0.08	6.7;0.05	6.7;0.05	6.70.02	6.7;0.01
145	4.8;0.06	4.4;0.05	4.4;0.03	4.4;0.03	4.4;0.01

Table 3. Spectral resolution (in Hz) of each number of trials.

Coupling freqs (Hz)	Number of trials				
	5	**15**	**30**	**50**	**100**
5	2	2	2	2	2
9	5	2	2	2	2
13	5	3	2	2	2
87	40	40	35	35	35
115	70	55	50	50	50
145	60	60	60	60	60

analysis considered significant if above the 95% confidence limits, calculated in section 2.3 for tPAC.

In this study, the rhythmic modulation of motor unit activity, which reflects contributions from rhythmic cortical activity, obtained from paired surface EMG recordings over the ankle flexor TA is acquired with the goal of studying and investigating neuronal coupling mechanisms associated with locomotion. Features from theta (4-8 Hz), alpha (8-12 Hz), low-beta (12-20 Hz), high-beta (20-30 Hz), and gamma (30-45 Hz) frequency bands were extracted and analysed to identify any modulations in the functional coupling of motor units during walking. tPAC analysis was therefore applied to the data with f_P and f_A frequency ranges of interest, $[4-8]$ Hz and $[8-50]$ Hz, respectively.

Examples of paired rectified EMG signals during treadmill walking at 4 km/h and time-frequency tPAC analysis from 3 subjects analysed from 30-, 50-, and 100-step cycles are shown in Fig. 5. Some features shown on individual estimates are common across all subjects as illustrated in Fig. 5(B)-(D). Time-frequency maps show that coupling strength encompasses not only frequency components of motor unit correlation between 8 Hz and 20 Hz [28, 29], but also higher frequencies (>30 Hz) at ∼0.8 s (around heel trigger). To summarise the correlation structure in group of subjects, the individual estimates are combined, or pooled, into a single representative estimate. Table 4 summarises the pooled estimates in different frequency bands. Although the results of tPAC present significant coupling in all frequency bands, it is worth noting that the coupling strength is concentrated in distinct frequency bands, showing peak values at $f_P \sim$ 6 Hz coupled to $f_A \sim$ 8-32 Hz. These strong coupling strengths are observed during late swing around heel contact (∼ 0.74-0.82 s). Here, tPAC analysis using 30-, 50-, and 100-step cycles are able to detect similar significant coupling in the time-frequency plane.

4. Conclusion

tPAC analysis is used to detect timing and frequencies of coupled oscillatory components: a slower oscillation (f_P) and a faster oscillation (f_A), where the amplitude of faster oscillations is coupled to the phase of slower oscillation. This study has reviewed relevant theoretical aspects of tPAC analysis using generalized Morse wavelets. A particular subset of the generalized Morse wavelets, Airy wavelets (γ=3), are used in this study because they have zero asymmetry in time domain and are nearly symmetric in the frequency domain [6, 8]. Optimal value of β depends upon the requirement of the analysis. tPAC method is more accurate in detecting the coupling for setting β to higher value, as seen in Section 3.1.

In Section 3.2, results from tPAC analysis of simulated dataset, with an emphasis on small numbers of trials (5, 15, 30, 50, and 100 trials), are obtained using Airy wavelet with $\beta = 27$. The results show that performances in coupling detection improved with increasing numbers of trials. Overall, the results from tPAC analysis using number of trials more than 15 trials offers better joint time-frequency resolution.

The method has been used to characterise the correlation structure in experimental data consisting of paired surface EMG signals during treadmill walking, as seen in Section 3.3. The main finding is that tPAC method is able to detect localised correlation in the time-frequency plane. Our results suggest that tPAC analysis gives useful information for investigation of non-stationary neuronal coupling mechanisms underlying human treadmill locomotion, which involve only short segments (or small numbers of steps) of EMG recordings. The results indicate that theta oscillation ($f_P \sim 6$ Hz) is strongly coupled to alpha and low-beta rhythms ($f_A \sim$ 8-20 Hz) during late swing. In addition, significant coupling is between ∼ 6 Hz and ∼ 20-45 Hz, specifically around heel contact. These frequency components partly overlap with the frequency

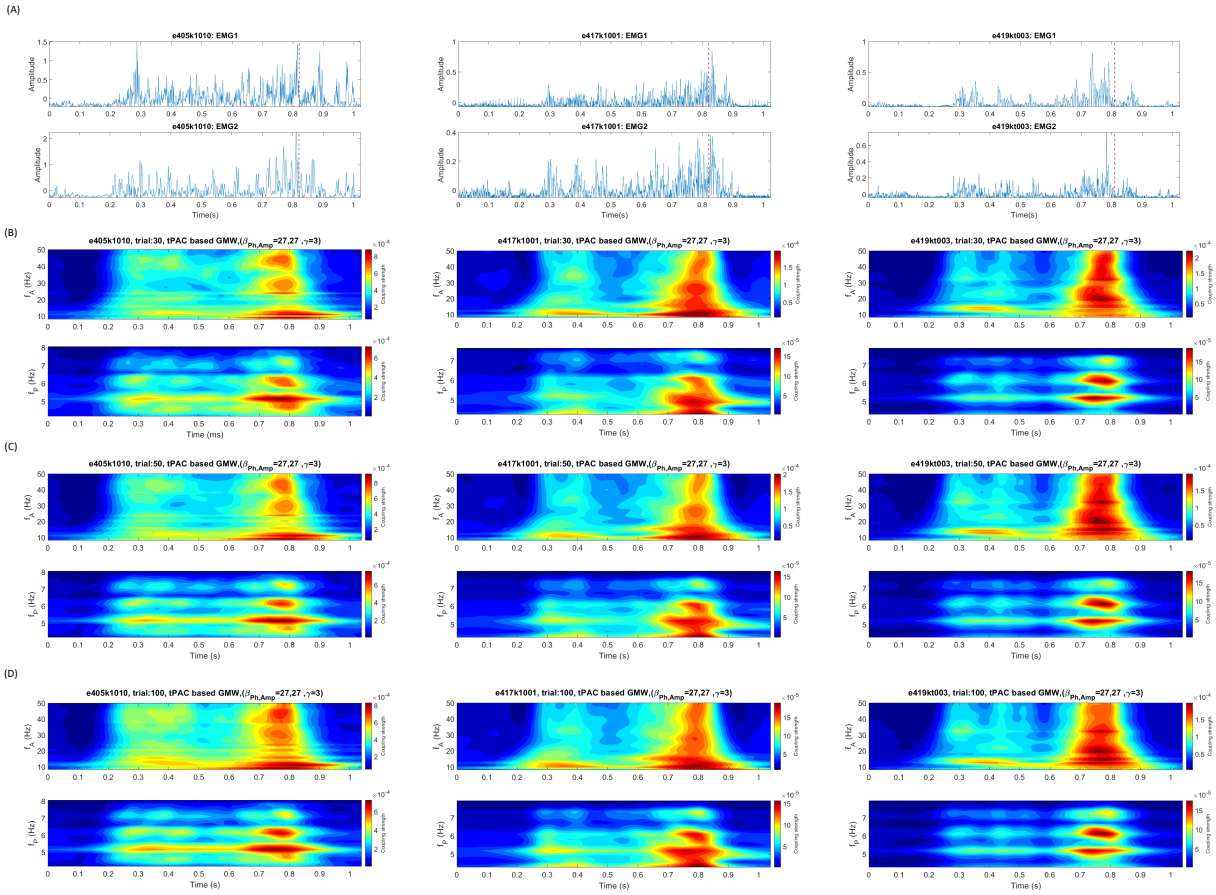

Figure 5: Examples of individual subjects analysed from 30-, 50-, and 100-step cycles, segmented into 1040 ms nonoverlapping epochs during treadmill walking. The time scale on time-frequency plots is labelled as 0-1.04 s, heel triggers are at 0.82 s. Columns represent records while rows represent (A) Examples of paired rectified surface EMG signals during treadmill walking, with dash red lines showing moments of heel strike. (B)-(D) Individual time-frequency tPAC maps analysed from 30-, 50, and 100-step cycles, respectively.

Table 4. Pooled peak time-frequency for tPAC analyses of all subjects during treadmill walking.

Frequency bands	Pooled tPAC estimates		
	30 trials	50 trials	100 trials
4-8 Hz	6 Hz, 0.75-0.79 s	6 Hz, 0.75-0.79 s	6 Hz, 0.75-0.79 s
8-12 Hz	8 Hz, 0.75-0.82 s	9 Hz, 0.78-0.79 s	9 Hz, 0.77-0.81 s
12-20 Hz	19 Hz, 0.74-0.79 s	19 Hz, 0.74-0.80 s	19 Hz, 0.74-0.80 s
20-30 Hz	24 Hz, 0.75-0.79 s	24 Hz, 0.76-0.79 s	24 Hz, 0.76-0.79 s
30-45 Hz	32 Hz, 0.77-0.80 s	32 Hz, 0.76-0.80 s	32 Hz, 0.76-0.80 s

ranges in the study of [30], who provide evidence in investigating the functional coupling between the motor cortex and TA muscles at 8-12 and 24-40 Hz in swing phase during treadmill walking. This finding is consistent with their suggestion that the motor cortex and the corticospinal tract contribute to the control of walking.

Although this study is constrained to EMG acquired during walking, this approach could be used to analyse EMG data from different walking speeds. Also, it is possible to apply tPAC analysis to other physiological data.

Acknowledgment

I wish to express my sincere gratitude to Dr. David M Halliday, University of York, for providing me very useful advices, guidance and explanations in both the fields of neuroscience and signal processing.

References

[1] J.-S. Brittain, C. Catton, B. Conway, J. Nielsen, N. Jenkinson, D. Halliday, Optimal spectral tracking-with application to speed dependent neural modulation of tibialis anterior during human treadmill walking, Journal of Neuroscience Methods 177 (2009) 334–347.

[2] D. Halliday, S. Farmer, On the need for rectification of surface EMG, Journal of Neurophysiology 103 (2010) 3547.
[3] D. Allen, C. Mackinnon, Time-frequency analysis of movement-related spectral power in eeg during repetitive movements: A comparison of methods, Journal of Neuroscience Methods 186 (2010) 107–115.
[4] F. Artoni, C. Fanciullacci, F. Bertolucci, A. Panarese, S. Makeig, S. Micera, C. Chisari, Unidirectional brain to muscle connectivity reveals motor cortex control of leg muscles during stereotyped walking, NeuroImage 159 (2017) 403–416.
[5] P. Grosse, M. Cassidy, P. Brown, EEG-EMG, MEG-EMG and EMG-EMG frequency analysis: physiological principles and clinical applications, Clinical Neurophysiology 113 (10) (2002) 1523–1531.
[6] J. Lilly, S. Olhede, On the analytic wavelet transform, IEEE Transactions on Information Theory 56 (2010) 4135–4156.
[7] J.-S. Brittain, D. Halliday, B. Conway, J. Nielsen, Singletrial multiwavelet coherence in application to neurophysiological time series, IEEE Transactionson Biomedical Engineering 54 (5) (2007) 854–862.
[8] J. Lilly, S. Olhede, Generalized morse wavelet as a superfamily of analytic wavelets, IEEE Transactions on Signal Processing 60 (11) (2012) 6036–6041.
[9] P. Wang, J. Gao, Extraction of instantaneous frequency from seismic data via the generalized morse wavelets, Journal of Applied Geophysics 93 (Supplement C) (2013) 83–92.
[10] L. Aguiar-Conraria, M. Soares, The continuous wavelet transform: moving beyond uni- and bivariate analysis, Journal of Economic Surveys 28 (2) (2014) 344–375.
[11] A. Nakhnikian, S. Ito, L. Dwiel, L. Grasse, G. Rebec, L. Lauridsen, J. Beggs, A novel cross-frequency coupling detection method using the generalized morse wavelets, Journal of Neuroscience Methods 269 (2016) 61–73.
[12] A. Tort, M. Kramer, C. Thorn, D. Gibson, Y. Kubota, A. Graybiel, N. Kopell, Dynamic cross-frequency couplings of local field potential oscillations in rat striatum and hippocampus during performance of a t-maze task, PNAS 105 (51) (2008) 20517–20522.
[13] A. Onslow, R. Bogacz, M. Jones, Quantifying phaseamplitude coupling in neuronal network oscillations, Progress in Biophysics and Molecular Biology 105 (1–2) (2011) 49–57.
[14] R. Canolty, C. Cadieu, K. Koepsell, K. R.T., J. Carmena, Multivariate phase-amplitude cross-frequency coupling in neurophysiological signals, IEEE Transactions on Biomedical Engineering 59 (1) (2012) 8–11.
[15] B. Voytek, M. D'Esposito, N. Crone, R. Knight, A method for event-related phase/amplitude coupling, NeuroImage 64 (2013) 416–424.
[16] A. Vaz, R. Yaffe, J. Wittig Jr, S. Inati, K. Zaghloul, Dual origins of measured phase-amplitude coupling reveal distinct neural mechanisms underlying episodic memory in the human cotex, NeuroImage 148 (2017) 148–159.
[17] W. Penny, E. Duzel, K. Miller, J. Ojemann, Testing for nested oscillation, Journal of Neuroscience Methods 174 (1) (2008) 50–61.
[18] A. Tort, R. Komorowski, H. Eichenbaum, N. Kopell, Measuring phase-amplitude coupling between neuronal oscillation of different frequencies, Journal of Neurophysiology 104 (4) (2010) 1195–1210.
[19] R. Canolty, R. Knight, The functional role of cross-frequency coupling, Trends in Cognitive Sciences 14 (11) (2010) 506–515.
[20] B. Pittman-Polletta, W.-H. Hsieh, S. Kaur, M.-T. Lo, K. Hu, Detecting phase-amplitude coupling with high frequency resolution using adaptive decompositions, Journal of Neuroscience Methods 226 (2014) 15–32.
[21] A. Dvorak, A. Fenton, Toward a proper estimation of phase-amplitude coupling in neural oscillations, Journal of Neuroscience Methods 225 (2014) 42–56.
[22] S. Samiee, S. Baillet, Time-resolved phase-amplitude coupling in neural oscillations, NeuroImage 159 (2017) 270–279.
[23] J. Lilly, S. Olhede, High-order properties of analytic wavelets, IEEE Transactions on Signal Processing 57 (1) (2009) 146–160.
[24] S. Olhede, A. Walden, Generalized morse wavelets, IEEE Transactions on Signal Processing 50 (11) (2002) 2661–2669.
[25] T. Özkurt, A. Schnitzler, A critical note on the definition of phase-amplitude cross-frequency coupling, Journal of Neuroscience Methods 201 (2) (2011) 438–443.
[26] J. Aru, J. Aru, V. Priesemann, M. Wibral, L. Lana, G. Pipa, W. Singer, R. Vicente, Untangling cross-frequency coupling in neuroscience, Current Opinion in Neurobiology 31 (2015) 51–61.
[27] D. Thengone, K. Gagnidze, D. Pfaff, A. Proekt, Phaseamplitude coupling in spontaneous mouse behavior, PLOS ONE 11 (9) (2016) 1–19.
[28] D. Halliday, B. Conway, Christensen, N. Hansen, N. Petersen, Nielsen, Functional coupling of motor units is modulated during walking in human subjects, Journal of Neurophysiology 89 (2003) 960–968.
[29] S. Suwansawang, D. Halliday, Time-frequency based coherence and phase locking value analysis of human locomotion data using generalized morse wavelets, in: Proceedings of the 10th International Joint Conference on Biomedical Engineering Systems and Technologies (BIOSTEC 2017) - Volume 4: BIOSIGNALS, Porto, Portugal, 2017, pp. 34–41.
[30] T. H. Petersen, M. Willerslev-Olsen, B. Conway, J. Nielsen, The motor cortex drives the muscles during walking in human subjects, The Journal of Physiology 590 (Pt 10) (2012) 2443–2452.